Federal Aviation
Administration

DOT/FAA/AM-21/5
Office of Aerospace Medicine
Washington, DC 20591

CARI Documentation: Radiation Transport in the Atmosphere

Kyle Copeland

Civil Aerospace Medical Institute
Federal Aviation Administration
Oklahoma City, OK 73125Location/Address

March 2021

Final Report

NOTICE

This publication and all Office of Aerospace Medicine technical reports are available in full-text from the Civil Aerospace Medical Institute's publications Web site: (www.faa.gov/go/oamtechreports)

Technical Report Documentation Page

1. Report No.	2. Government Accession No.	3. Recipient's Catalog No.
DOT/FAA/AM-21/5		

4. Title and Subtitle	5. Report Date
CARI-7 DOCUMENTATION: RADIATION TRANSPORT IN THE ATMOSPHERE	March 2021
	6. Performing Organization Code
7. Author(s)	8. Performing Organization Report No.
Copeland, K.	
9. Performing Organization Name and Address	10. Work Unit No. (TRAIS)
Civil Aerospace Medical Institute FAA	
	11. Contract or Grant No.
12. Sponsoring Agency name and Address	13. Type of Report and Period Covered
Office of Aerospace Medicine Federal Aviation Administration 800 Independence Ave., S.W. Washington, DC 20591	
	14. Sponsoring Agency Code
15. Supplemental Notes	

16. Abstract

Primary cosmic radiation from both the Sun and interstellar space enters Earth's atmosphere in varying amounts. Outside of Earth's atmosphere, cosmic radiation is modulated by solar activity and Earth's magnetic field. Once the radiation enters Earth's atmosphere, it interacts with Earth's atmosphere in the same manner regardless of its point of origin (solar or galactic). CARI (i.e., the Civil Aviation Research Institute—the previous name of what is now the Civil Aerospace Medical Institute, or CAMI) software for calculating doses of ionizing radiation in the atmosphere from cosmic radiation has been in development at CAMI since the late 1980s. For CARI-6 and earlier versions, the approach used to calculate time- and location-dependent dose rates in the atmosphere consisted of interpolation from databases of precalculated galactic cosmic radiation dose rates covering a wide range of input conditions (latitude, longitude, solar activity, and altitude). These early databases were not appropriate for the calculation of solar proton event dose rates. They were also limited to 87,000 feet maximum altitude and increasingly inaccurate for effective doses at altitudes above 60,000 feet. This report presents the methods of calculating the cosmic radiation particle fluxes and doses in the atmosphere used in CARI-7 and -7A. The approach consists of building representative cosmic radiation shower contributions from a database of precalculated Monte Carlo simulations of particle entry into Earth's atmosphere. While somewhat slower than the older method, the new approach improves accuracy at high altitudes and is easily applied to galactic cosmic radiation and solar particle events. While CARI-7 handles the data in the most consistent with the Monte Carlo simulations, CARI-7A offers added options for users in handling these data.

17. Key Words	18. Distribution Statement
Ionizing Radiation, Cosmic Radiation, Radiation Transport, Software, CARI-7, CARI-7A, Dosimetry, Aircrews.	Document is available to the public through the Internet: http://www.faa.gov/go/oamtechreports/

19. Security Classif. (of this report)	20. Security Classif. (of this page)	21. No. of Pages	22. Price
Unclassified	Unclassified	30	

ACKNOWLEDGMENTS

The author gives special thanks to Herbert Sauer for his suggestion of the general approach used to apply Monte Carlo results to cosmic rays in the general way described in this report two decades ago, while we were developing the FAA's Solar Radiation Alert System, which was a proving ground for techniques later used in CARI-7. This work is in partial fulfillment of Project 2017-AAM-631-NUM-10114 sponsored by the FAA's Office of Aerospace Medicine.

CONTENTS

LIST OF ABBREVIATIONS

ACE	Advanced Composition Explorer
CARI	Civil Aviation Research Institute
CAMI	Civil Aerospace Medical Institute
CR	cosmic radiation
FLUKA	FLUktuierende KAskade
GEANT4	GEometry ANd Tracking 4
GCR	galactic cosmic radiation
ICRP	International Commission on Radiological Protection
ICRU	International Commission on Radiation Units and Measurements
ISO	International Standards Organization
MCNP	Monte Carlo N-Particle
MCNPX	Monte Carlo N-Particle eXtended
NASA	National Aeronautics and Space Administration
NCRP	National Council on Radiation Protection and Measurement
NOAA	National Oceanic and Atmospheric Administration
PHITS	Particle and Heavy Ion Transport
SCR	solar cosmic radiation
SEP	solar energetic particle
SST	supersonic transport

EXECUTIVE SUMMARY

Primary cosmic radiation from both the Sun and interstellar space enters Earth's atmosphere in varying amounts. Outside of Earth's atmosphere, cosmic radiation is modulated by solar activity and Earth's magnetic field. Once the radiation enters Earth's atmosphere, it interacts with Earth's atmosphere in the same manner regardless of its point of origin (solar or galactic). CARI (i.e., the Civil Aviation Research Institute—the previous name of what is now the Civil Aerospace Medical Institute, or CAMI) software for calculating doses of ionizing radiation in the atmosphere from cosmic radiation has been in development at CAMI since the late 1980s. For CARI-6 and earlier versions, the approach used to calculate time- and location-dependent dose rates in the atmosphere consisted of interpolation from databases of precalculated galactic cosmic radiation dose rates covering a wide range of input conditions (latitude, longitude, solar activity, and altitude). These early databases were not appropriate for the calculation of solar proton event dose rates. They were also limited to 87,000 feet maximum altitude and increasingly inaccurate for effective doses at altitudes above 60,000 feet. This report presents the methods of calculating the cosmic radiation particle fluxes and doses in the atmosphere used in CARI-7 and -7A. The approach consists of building representative cosmic radiation shower contributions from a database of precalculated Monte Carlo simulations of particle entry into Earth's atmosphere. While somewhat slower than the older method, the new approach improves accuracy at high altitudes and is easily applied to galactic cosmic radiation and solar particle events. While CARI-7 handles the data in the most consistent with the Monte Carlo simulations, CARI-7A offers added options for users in handling these data.

CARI Documentation: Radiation Transport in the Atmosphere

INTRODUCTION

Particle Sources

The atoms we typically encounter on the surface of the Earth are not very energetic. For example, air molecules are moving about as fast as bullets and jet aircraft. These are energies of a few hundredths of an electron volt (eV). At such low energies, any reaction that occurs is likely a chemical reaction, and nuclear reactions are rare. For comparison, in Earth's magnetosphere, auroral electrons typically have 1000 to 10,000 eV (1 to 10 keV), while in Earth's inner trapped radiation belt, protons typically have 10,000,000 to 100,000,000 eV (10 to 100 MeV). Particles of yet higher energies come from outer space with much more energy than even the trapped particles found in the magnetosphere.

These particles from outside Earth's immediate sphere of influence are known as *cosmic rays* or *cosmic radiation* (CR). CR is typically subcategorized into two categories: galactic cosmic radiation (GCR) and solar cosmic radiation (SCR; also called solar energetic particle [SEP] radiation). They are of similar elemental composition (as the Sun is to the rest of the galaxy), but SCR is of much lower average energy, has a much more variable intensity, and is more variable in heavier element flux. Bursts of >1 GeV SEPs are very infrequent and difficult to predict. Therefore, most of the time, the interplanetary CR composition is dominated by GCR, which varies with solar activity and roughly consists of about 85% protons, 14% α-particles, and 1% heavier nuclei. Table 1 shows the relative elemental abundances of hydrogen through nickel in GCR as measured by instruments on the Advanced Composition Explorer (ACE) satellite (National Aeronautics and Space Administration [NASA], 1999).

Table 1

Relative Abundance of Elements (Si = 100) in GCR as Measured by ACE

Atomic Number	GCR Abundance	Estimated Error	Atomic Number	GCR Abundance	Estimated Error
1	3.20E+05	6.00E+03	15	3.30E+00	3.00E-01
2	2.70E+04	5.80E+02	16	1.75E+01	8.00E-01
3	1.36E+02	3.00E+00	17	3.20E+00	3.00E-01
4	5.07E+01	2.80E+00	18	7.00E+00	4.00E-01
5	1.82E+02	5.50E+00	19	4.90E+00	4.00E-01
6	7.26E+02	1.34E+01	20	1.24E+01	6.00E-01
7	1.87E+02	4.60E+00	21	2.30E+00	3.00E-01
8	7.13E+02	1.17E+01	22	1.06E+01	5.00E-01
9	1.13E+01	8.00E-01	23	5.00E+00	3.00E-01
10	1.03E+02	2.50E+00	24	9.60E+00	5.00E-01

Atomic Number	GCR Abundance	Estimated Error	Atomic Number	GCR Abundance	Estimated Error
11	1.86E+01	9.00E-01	25	5.90E+00	4.00E-01
12	1.36E+02	2.70E+00	26	7.43E+01	1.40E+00
13	1.85E+01	8.00E-01	27	4.00E-01	1.00E-01
14	1.00E+02	2.00E+00	28	3.50E+00	3.00E-01

Note. GCR = Galactic cosmic radiation; ACE = Advanced Composition Explorer. Adapted from "ACE abundance data to plot" (Website), by NASA, 1999, (helios.gsfc.nasa.gov/ace/abund_plot.html).

Particle Interactions in Earth's Atmosphere

Near the Earth's surface, the heaviest elements present in primary CR are practically nonexistent because they generally collide with atoms and molecules at higher altitudes in the atmosphere, producing a *shower* of high-speed *secondary* particles (Figure 1). The energies of CR particles when they arrive at Earth can be $>10^{20}$ eV. While the atmosphere shields the surface as effectively as approximately 10 meters of water, CR-generated secondary particles still manage to reach the surface (e.g., the neutrinos usually pass through the whole Earth). A CR particle at the top of the energy range can produce a shower in the atmosphere (Figure 1) with millions of secondary particles, covering many acres.

Figure 1.

Collision between a High-Energy Cosmic Ray Particle and an Atom Imaged in a Photographic Emulsion, as Viewed through a Microscope

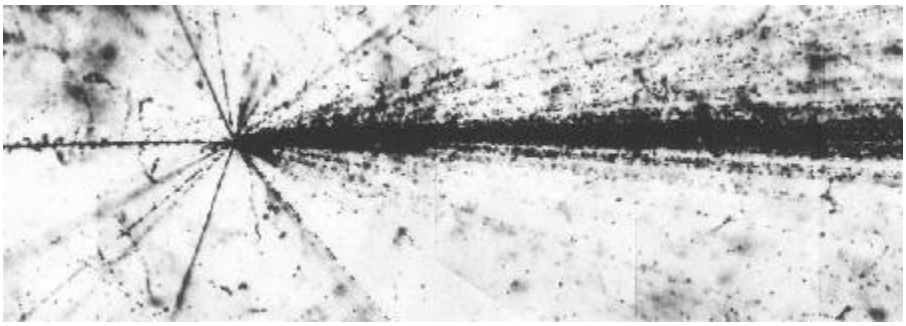

Note. This image is typical of photographic plates lifted by helium balloons to near the top of the atmosphere to record CR particles' passage. Particles are identified based on the thickness of the tracks they made. This method showed the particles to be ions of normal matter (i.e., mostly hydrogen, some helium, and lesser amounts of heavier elements). From "#33 Cosmic Rays," D.P. Stern and M. Peredo, 2005, www-spof.gsfc.nasa.gov/Education/wcosray.html. In the public domain.

All particles in the CR shower produced from the first and resulting interactions due to the entrance of the primary CR are often lumped together and called secondary CR. The secondary shower is a host of subatomic particles and nuclear fragments (Figure 2). The remains of the impacting CR particle and the secondary particles generated in the initial collision often have enough energy to create more secondary CR particles. The secondary particle population increases until the processes are no longer energetic enough to result in a net gain in secondary particle population as the secondaries interact with the atmosphere. Thus, when CR enters the atmosphere, the number of secondary particles initially increases with decreasing altitude, reaches a maximum, and decreases with further reductions in altitude, all while continuously changing in composition and energy. As it approaches the Earth, the primary GCR is essentially isotropic

(i.e., the same from all directions), but the radiation in the atmosphere becomes increasingly anisotropic at lower altitudes due to slant-depth effects (i.e., showers coming from the sides pass through more atmosphere than showers coming from above) and the presence of the Earth.

Figure 2

Evolution of a Cosmic Ray Shower

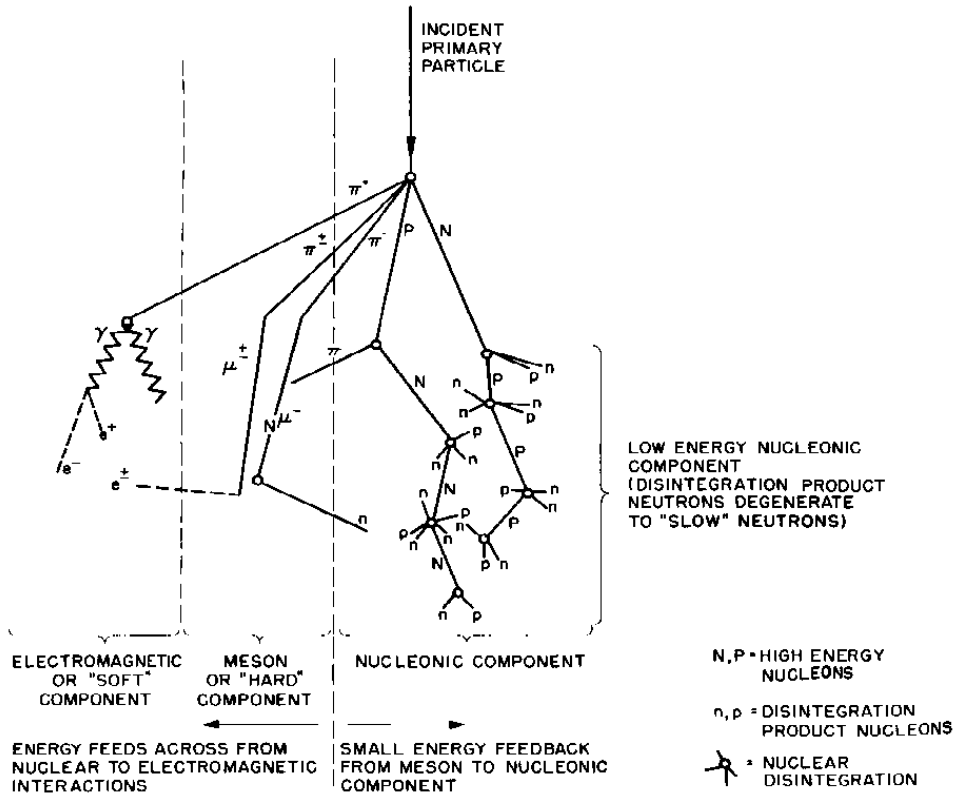

Schematic Diagram of Cosmic Ray Shower

Note. From https://www.ngdc.noaa.gov/stp/image/shower.gif. In the public domain.

Incident primary CR particles interact with atmospheric nuclei through nuclear and electromagnetic forces. If a CR particle has at least an energy level of a few GeV, there is sufficient energy to produce pi-mesons and other secondary CR particles in the collisions. As previously mentioned, energetic primaries, primary fragments, and the secondary particles continue to propagate in the atmosphere and produce more secondary particles along their trajectories. For example, a typical primary GCR proton entering with a vertical trajectory has an average of 12 nuclear interactions before it reaches sea level, corresponding to an interaction mean free path (λ) in the air of about 80 $g \cdot cm^{-2}$. Because larger nuclei have larger nuclear collision cross-sections than protons (thus, much shorter mean free paths), their first nuclear interactions tend to occur at higher altitudes. Figure 3 shows the nuclear interaction mean free path as a function of projectile mass number in the air. For iron, this is only about 13 $g \cdot cm^{-2}$. Because most of the heavy nuclei in the primary CR are fragmented in the first interaction, there is virtually no chance of a heavy ion making it to sea level.

In addition to nuclear fragments and nucleons, primary CR interactions produce mesons. The most important of these are the pi-mesons (also called pions). Charged and neutral pions are produced in a ratio of about 2:1. The neutral pions have extremely short lifetimes and usually decay into two gamma rays, starting electromagnetic cascades. The charged pions have much longer lifetimes and can often interact instead of decaying. The odds of interaction are dependent upon the pion's energy and density of the atmosphere. Due to time dilation effects, very high energy charged pions almost exclusively interact. The low energy pions decay into muons and mu-neutrinos. Interaction becomes more likely as the cascade travels deeper into the atmosphere, where the atmosphere has a greater density. Those muons that do not decay immediately mostly lose energy by ionization. The energy loss for muons is near 2 MeV per $g \cdot cm^{-2}$. Muon decay into electrons, positrons, and neutrinos, and are the most numerous energetic charged particles arriving at sea level, with a flux of about 1 muon per $cm^2 \cdot s^{-1}$.

Figure 3

Interaction Mean Free Path, λ, for High-Energy Nuclear Interactions in Air

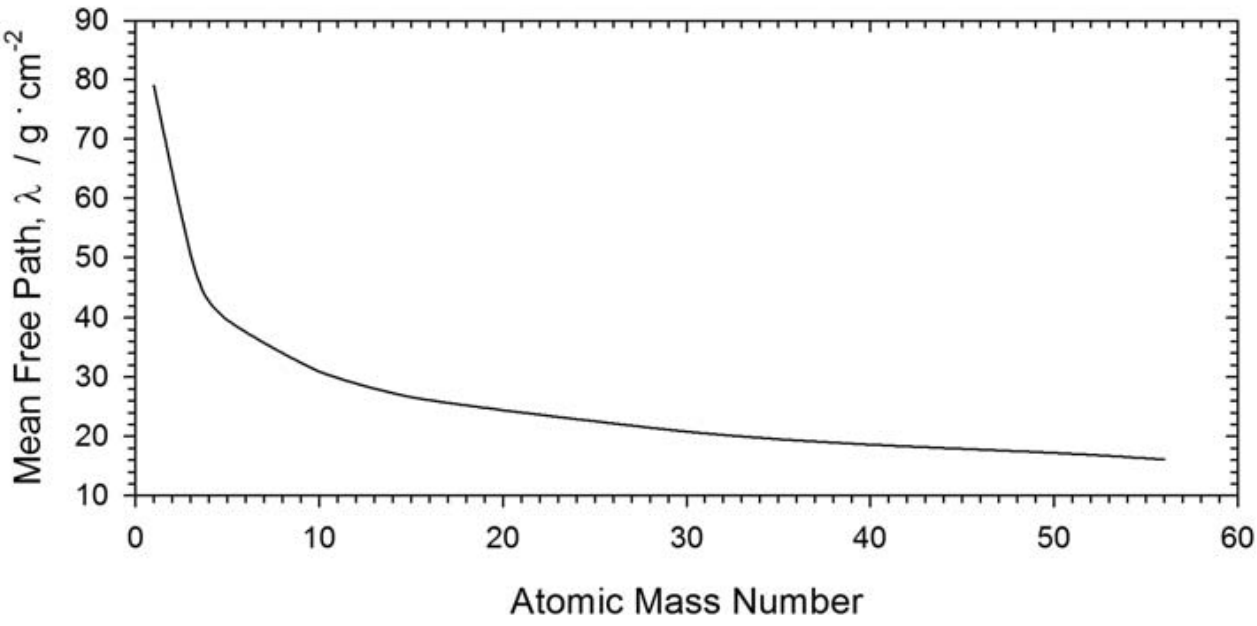

Note. Adapted from "Cosmic Ray Particle Fluences in the Atmosphere Resulting from Primary Cosmic Ray Heavy Ions and Their Resulting Effects on Dose Rates to Aircraft Occupants as Calculated with MCNPX 2.7.0" by K. A. Copeland, 2014, A doctoral thesis at the Royal Military College of Canada (RMCC): available from the Massey Library collection at RMCC and the Canadian National Archives in Ottawa, Canada.

Another important process is the electromagnetic *cascade*, which can begin when a gamma-ray photon (e.g., from meson decay) passes close to an atom's nucleus. Because of the photon's electromagnetic nature, it may interact with the electric field of the nucleus and create an electron-positron pair. The energy required for pair production is just over 1 MeV. The initiating photon can have one thousand or more times that energy, and hence, the electron-positron pair produced can be very fast-moving. If fast-moving electrons and positrons pass close to atomic nuclei, they will accelerate (i.e., change speed and direction) due to the influence of positive electric charge of the protons in the nucleus. An accelerated charged particle will emit a photon to conserve momentum, so the accelerations can produce more photons capable of

producing more electron-positron pairs. Eventually, the original gamma-ray energy is converted into many lower-energy photons, electrons, and positrons.

The above is not a complete description but should be viewed as a very brief introduction to some of the physical processes that must be considered when attempting to calculate CR dose rates in Earth's atmosphere. The field of study is now over 100 years old. Many books and websites describe CR in Earth's atmosphere, including important nuclear and atomic physics.

Noncosmic Sources of Radiation in Aerospace Environments

Air and space travelers are constantly exposed to GCR. Other human-made and natural sources can result in higher doses rates for short periods, depending on the specific environment and time of exposure. SCR (i.e., CR from the Sun) is a natural source. Other natural sources include lightning, terrestrial gamma-ray flashes, and trapped particles from Earth's radiation belts (a severe potential hazard for space vehicle crews). Human-made sources include radioactive cargo (e.g., medical isotopes), fallout from nuclear weapons testing, and releases of radioactivity into the atmosphere from nuclear reactors, such as those resulting from an operational accident or natural disaster.

CARI Software

CARI (i.e., the Civil Aviation Research Institute—the previous name of what is now the Civil Aerospace Medical Institute, or CAMI) software for calculating doses of ionizing radiation in the atmosphere from CR has been in development at CAMI the since the late 1980s. The sixth-generation family of CARI programs (CARI-6, -6M, -6P, -6PM, and 6W, hereafter referred to collectively as CARI-6) is well proven at aviation altitudes and used for aircrew dosimetry in many countries. However, in the uppermost atmosphere, CARI-7 is more accurate because of its superior nuclear breakup modeling. In CARI-6, all primary nuclei were broken apart before transport through the atmosphere, while in CARI-7, the primary nuclei and intermediate-mass fragments were tracked as the nuclear cascade moved through the atmosphere.

To calculate a CR dose rate at any point in the atmosphere for any date and time, two questions must be answered: (a) what CR spectra are entering at the top of the atmosphere for any given day and time, and (b) what dose rate results from the answer to the first question for that day and time for the location in the atmosphere under consideration. In CARI-7, these problems are solved independently. In the first two CARI-7 documentation reports, the methods used to arrive at the incident CR spectrum entering Earth's atmosphere are discussed (Copeland, in press-a, in press-b). This report, the third in the CARI-7 documentation series, describes the methods used to convert incident CR spectra at the top of the atmosphere to dose rates of various sorts throughout the atmosphere in all variants of CARI-7.

There are two publically available versions of CARI-7, -7 and -7A (Copeland, 2014, 2017a). User feedback indicated the number of options was impractical for users who simply wanted to upgrade from CARI-6 to the newer transport data. Development was thus divided into two branches, -7 and -7A. For CARI-7A, most options are now included as user choices, while for CARI-7, many options are preset to what was deemed the most reasonable choice for users to minimize transition problems when they upgrade from CARI-6 to the more capable CARI-7.

DESCRIPTION

Primary Particles

For radiation effects, primary nuclides up to and including iron are considered potentially significant sources of biological dose in interplanetary space (Lei et al., 2009). Lei et al. calculated dose and dose equivalent behind a shield of 1 $g \cdot cm^{-2}$ polyethylene to an occupant of a spacecraft, finding that protons would contribute almost 60% of the absorbed dose from GCR only approximately 20% of the dose equivalent. Heavy nuclei were found to be important contributors because of their greater relative biological effectiveness (i.e., more biological damage form the same physical dose). As is evident from Figure 1, the effective dose calculated without using the superposition approximation is much greater, emphasizing the importance of the heavy ion contribution at high altitudes in the atmosphere.

For CARI-7 and -7A, the general-purpose Monte Carlo radiation transport program MCNPX 2.7.0 (Oak Ridge National Laboratory, 2011) developed at Los Alamos National Laboratory was used to simulate showers originating from GCR primary ions traveling into Earth's atmosphere. Chosen primary particles were selected based on their expected importance to biological dose rates in the atmosphere over the energy range recommended by the MCNPX developers (M. James, personal communication, 2012). Consultations with MCNPX developers indicated that while the Los Alamos Quark-Gluon String Model module in MCNPX can transport heavy ions at energies up to 1 TeV per nucleon, results were deemed untrustworthy above 1 TeV. This is because proton and neutron transport is not verified at energies beyond 1 TeV, and many of the secondary products are also not well-modeled near these energies; for instance, photon and electron models begin extrapolating at 50 GeV. Also, particles that are not transported deposit their energies locally in MCNPX.

Particle Transport

Particle transport through the model atmosphere (see Section “Earth’s Atmosphere”) was simulated using a 1, 2, 5… grid of primary particle entry energies ranging from 1 MeV to 1 TeV. For all showers, particles tracked in MCNPX were kaons, pions, muons, photons, electrons, neutrinos, neutrons, protons, deuterons, tritons, helions, alphas, and other atomic nuclei up to iron. Fluence tallies were kept for dosimetry analysis at each tally altitude for all these particles except kaons, neutral pions, and neutrinos. Preliminary calculations indicated no significant direct contribution to these particles' effective dose, presumably due to their short lives (kaons and neutral pions) or low interaction cross-section (neutrinos). Particles that passed through the lowest layer of the model atmosphere and interacted with the water sphere below it were allowed to return and to generate secondary particles that returned to the atmosphere. Particles that exited the atmosphere through the uppermost surface were considered lost.

Simulation Numbers

The number of simulations for each ion at each energy that would be needed was a significant consideration. The overall desire was to achieve a standard uncertainty of a few percent or less in the effective dose rate calculations, assuming independence of all uncertainties. Thus, an attempt was made to minimize uncertainty in the secondary particle fluxes per incident primary particle. Table 2 shows the minimum number of trials (simulated showers) used to assemble an average shower at each energy.

Table 2

Minimum Number of Trials Used to Generate the Isotropic Shower Data for Each Ion Energy

Energy/MeV	No. of trials	Energy/MeV	No. of trials
1E+00 through 5E+03	1E+08	1E+04, 2E+04, and 5E+04	1E+07
1E+05	1E+06	2E+05	6E+05
5E+05	3E+05	1E+06	1E+05

The minimum number of showers for each ion at each energy was set in the following manner: Proton and iron showers of the same energy were simulated until doubling the number of showers no longer resulted in a significant drift of the values of the flux tallies for protons or iron ions at the same energy, 10^8 showers were simulated, or approximately 200,000 core hours were used in calculations. If the estimated time to 10^8 showers was less than 24 hours on 252 CPU cores, then 10^8 showers were used even if the convergence goal was exceeded. At least 100,000 showers were simulated even for the highest energy particles.

The large number of shower simulations required millions of CPU core hours. The following high-performance computing facilities were utilized: Compute Canada's HPCVL (High-Performance Computing Virtual Laboratory), the U.S. National Oceanic and Atmospheric Administration's (NOAA) "JET" high-performance computing system, and the FAA's HiPARCoS (High-Performance Aeromedical Research Computing System).

Earth's Atmosphere

Earth's atmosphere (see Appendix A for an overview) provides a great deal of shielding to everything on the ground beneath it, equivalent to approximately 10 m of water. The amount of shielding (i.e., the matter between someone in a vehicle and outer space) decreases rapidly as altitude increases. The model atmosphere used in CARI-7 is based on the 1976 U.S. Standard Atmosphere that was also used in earlier work on SCR (NOAA et al., 1976; Copeland et al., 2008). The 1976 U.S. Standard Atmosphere is an idealization of the steady-state atmosphere for moderate solar activity. Some properties of the CARI-7 model atmosphere are shown in Table 3 (p. 8).

The model atmosphere used in the MCNPX shower simulations differed from the standard in that the total distance from the vacuum of outer space (0 $kg \cdot m^{-3}$) to sea level was forced to be 100 km (328,000 ft), and below the lowest atmospheric shell, the Earth was modeled as a sphere of liquid water of radius 6371 km and density 10^3 $kg \cdot m^{-3}$ (1 $g \cdot cm^{-3}$). The model atmosphere was divided into 1-km deep spherical shells. For each shell except the uppermost, density from the standard at the geopotential altitude halfway point through the shell was assigned to the whole shell, with all the remaining material above 99 km included in the uppermost shell. The resulting model was 100 km deep, with a total vertical column depth of 1035.1 $g \cdot cm^{-2}$. When using the shower data produced in this model atmosphere to calculate other quantities (e.g., dose rates), particle flux data are ordered and interpolated using depth rather than altitude. An altitude of 100 km is commonly accepted as the altitude of transition between outer space and Earth's atmosphere, known as the *Kármán Line*. Above this altitude, the atmosphere becomes too thin for conventional aircraft to maintain flight and aerodynamic control using surface effects. For incident radiation

Table 3

Shells of the Model Atmosphere Used in CARI-7

Shell	Depth / g · cm^{-2}	Density / kg · m^{-3}	Shell	Depth / g · cm^{-2}	Density / kg · m^{-3}	Shell	Depth / g · cm^{-2}	Density / kg · m^{-3}
1[A,B]	1.0351E+03	1.1673E+00	35	6.8477E+00	9.1468E-03	69	7.3214E-02	1.0195E-04
2	9.1835E+02	1.0581E+00	36	5.9330E+00	7.8367E-03	70	6.3019E-02	8.8804E-05
3[B]	8.1254E+02	9.5695E-01	37	5.1494E+00	6.7266E-03	71	5.4139E-02	7.7223E-05
4	7.1685E+02	8.6340E-01	38	4.4767E+00	5.7842E-03	72	4.6416E-02	6.7037E-05
5	6.3051E+02	7.7704E-01	39[B]	3.8983E+00	4.9835E-03	73	3.9713E-02	5.7951E-05
6[B]	5.5280E+02	6.9747E-01	40	3.3999E+00	4.2992E-03	74	3.3918E-02	4.9975E-05
7	4.8306E+02	6.2431E-01	41	2.9700E+00	3.7160E-03	75[B]	2.8920E-02	4.3040E-05
8	4.2063E+02	5.5719E-01	42	2.5984E+00	3.2211E-03	76	2.4616E-02	3.7016E-05
9[B]	3.6491E+02	4.9576E-01	43	2.2763E+00	2.7896E-03	77	2.0915E-02	3.1792E-05
10	3.1533E+02	4.3966E-01	44	1.9973E+00	2.4228E-03	78	1.7735E-02	2.7267E-05
11	2.7137E+02	3.8857E-01	45	1.7551E+00	2.1074E-03	79	1.5009E-02	2.3353E-05
12[B]	2.3251E+02	3.3743E-01	46	1.5443E+00	1.8358E-03	80	1.2673E-02	1.9971E-05
13	1.9877E+02	2.8838E-01	47	1.3607E+00	1.6016E-03	81	1.0676E-02	1.7054E-05
14	1.6993E+02	2.4646E-01	48	1.2006E+00	1.4013E-03	82	8.9708E-03	1.4540E-05
15[B]	1.4528E+02	2.1066E-01	49	1.0604E+00	1.2374E-03	83	7.5168E-03	1.2378E-05
16	1.2422E+02	1.8006E-01	50	9.3670E-01	1.0928E-03	84	6.2790E-03	1.0521E-05
17	1.0621E+02	1.5391E-01	51[B]	8.2742E-01	9.6503E-04	85	5.2269E-03	8.9282E-06
18[B]	9.0819E+01	1.3157E-01	52	7.3092E-01	8.5305E-04	86	4.3341E-03	7.5641E-06
19	7.7662E+01	1.1248E-01	53	6.4561E-01	7.6061E-04	87[B]	3.5777E-03	6.3660E-06
20	6.6414E+01	9.6157E-02	54	5.6955E-01	6.7741E-04	88	2.9411E-03	5.3280E-06
21[B]	5.6798E+01	8.2052E-02	55	5.0181E-01	6.0260E-04	89	2.4083E-03	4.4600E-06
22	4.8593E+01	6.9881E-02	56	4.4155E-01	5.3541E-04	90	1.9623E-03	3.7340E-06
23	4.1605E+01	5.9563E-02	57	3.8801E-01	4.7513E-04	91	1.5889E-03	3.1260E-06
24[B]	3.5648E+01	5.0807E-02	58	3.4050E-01	4.2112E-04	92	1.2763E-03	2.6160E-06
25	3.0568E+01	4.3372E-02	59	2.9838E-01	3.7276E-04	93	1.0147E-03	2.1880E-06
26	2.6231E+01	3.7052E-02	60	2.6111E-01	3.2953E-04	94	7.9588E-04	1.8280E-06
27[B]	2.2525E+01	3.1678E-02	61	2.2816E-01	2.9093E-04	95	6.1308E-04	1.5620E-06
28	1.9358E+01	2.7103E-02	62	1.9906E-01	2.5649E-04	96	4.5688E-04	1.2730E-06
29	1.6647E+01	2.3206E-02	63[B]	1.7341E-01	2.2582E-04	97	3.2958E-04	1.0610E-06
30[B]	1.4327E+01	1.9883E-02	64	1.5083E-01	1.9853E-04	98	2.2348E-04	8.8420E-07
31	1.2338E+01	1.7049E-02	65	1.3098E-01	1.7429E-04	99	1.3506E-04	7.3670E-07
32	1.0633E+01	1.4629E-02	66	1.1355E-01	1.5278E-04	100[B]	6.1390E-05	6.1390E-07
33[B]	9.1705E+00	1.2532E-02	67	9.8271E-02	1.3372E-04			
34	7.9173E+00	1.0696E-02	68	8.4899E-02	1.1685E-04			

[A] Tally surface at the inner and outer surfaces of this shell.

[B] Tally surface at the outer surface of this shell.

in CARI-7, the primary particles begin interacting with the atmosphere at this altitude. In CARI-7A, only vehicle shielding is effective above this altitude.

The Earth as a Shield

When summing secondary particle fluxes from incident CR, the Earth is considered an impenetrable shield that blocks the approach of radiation from all angles below the local horizon. The angle from a vehicle to the local horizon is calculated based on its altitude above mean sea level. For calculation of this angle, locations such as airports below sea level are treated as if they were at sea level.

Fluence to Dose Conversion

Background

Fluence to dose conversion coefficients were used to convert secondary particle fluences calculated by MCNPX at the tally surface atmospheric depths to desired dose types per incident particle. For CARI-7 release 4.0.2, in addition to total particle fluence, the doses available are International Commission on Radiological Protection (ICRP) Pub. 103 effective dose, ICRP Pub 60 effective dose, ambient dose equivalent H*(10), whole-body average absorbed dose, absorbed dose in 0.3-mm thick silicon, absorbed dose in 0.5-mm thick silicon, and un-normalized BF_3 neutron monitor tube counts.

For each of the eight output types in the model, the spectrum of each secondary except for neutrons and photons at each altitude is broken up into 100 separate energy bins spanning from <1 MeV to 1 TeV. Neutron and photon spectra are split into high- and low-energy subspectra, each subspectra having 99 unique bins and one bin of overlap with the spectrum of the other energy region at 1 MeV spanning from <10 eV to 1 TeV. For each bin, a characteristic energy is chosen using log-linear interpolation across the bin width, and a fluence-to-dose conversion coefficient is interpolated from a table of such values. The contribution from each bin is then summed. Outside the range of particle energies of published coefficients, linear extrapolation from the closest two published coefficients is used, with a minimum value of 10^{-16}.

Caveats

There are some limitations to this method. In outer space, away from the Earth, radiation is incident practically isotropically, but for aviation, a more realistic standard exposure geometry for GCR would be isotropic-from-above (Ferrari and Pelliccioni, 2003). Large sets of coefficients of this sort have not yet been calculated. Large sets useful for aviation cosmic ray dosimetry only exist in the isotropic, posterior-anterior, and anterior-posterior exposures (Pelliccioni, 2000; Sato et al., 2009, 2010; ICRP 2010). Of these geometries, isotropic exposure is the best match, usually showing very little difference when compared to isotropic-from-above coefficients.

Not all kinds of coefficients were robustly calculated for all altitudes since complete coefficient sets were not always available. The next subsections briefly describe the calculation of the various dose kinds. The needed fluence to dose conversion coefficients were either taken from the literature, calculated from data available from literature associated websites or calculated from data acquired by request from the authors (Pelliccioni, 2000; Sato et al., 2003a, 2010; Ferrari et al., 2005; Matthiä et al., 2018). Currently, there is no single set of such data for these particles for any of the dose endpoints that span the energy range needed for CARI-7. Hence, data from multiple sources were combined. Table 4 shows sources for each particle for each dose endpoint.

Table 4

Source Data for Fluence-to-Dose Conversion Coefficients

Particle or Nucleus	Ambient Dose Equiv. (H*(10))	Whole Body Absorbed dose[1]	ICRP Pub 60 Effective dose	ICRP Pub. 103 Effective dose	Absorbed dose in 0.3mm Si	Absorbed dose in 0.5mm Si	Count rate in NM-64 BF3 tube
Neutrons	P	S	P	I, S	M	M	M
Photons	P	P	P	I, P	M	M	-
Electrons	P	P	P	I, P	M	M	-
Positrons	P	P	P	I, P	M	M	-
Pos. Muons	P	P	P	I, P	M	M	M
Neg. Muons	P	P	P	I, P	M	M	M
Pos. Pions	P	P	P	I, P	M	M	M
Neg. Pions	P	P	P	I, P	M	M	M
Protons	P	S	P	I, S	M	M	M
Deuterons	E_{103}	S	S[2]	I, S	M	M[3]	-
Tritons	E_{103}	S	S[2]	I, S	M	M[3]	-
Helions	E_{103}	S	S[2]	I, S	M	M[3]	-
Alphas	E_{103}	S	S[2]	I, S	M	M[3]	-
Lithium-Iron	E_{103}	S	S[1]	I, S	M	M[3]	-

P – From Pelliccioni (2000): organ doses by request (M. Pelliccioni, personal communication, 2005).

E_{103} – Uses ICRP Pub. 103 fluence-to-effective dose coefficients.

S – From Sato et al. (2003a, 2009, 2010): organ doses available at phits.jaea.go.jp/ddcc/

I, X – Within the energy range of published data, coefficients are from ICRP Pub. 116, otherwise from X, where X is S or P as indicated.

M – D. Matthiä (personal communication, 2018).

[1] Based on organ-absorbed doses used in effective dose coefficients.

[2] For these particles, some ICRP Pub. 60 data are converted from ICRP Pub. 103 data.

[3] Set is incomplete; coefficients from 0.3-mm set are used as needed.

For ICRP Pub. 103 effective dose, coefficients from ICRP Pub 116 are used when possible. Outside of the energy ranges of the tables in ICRP Pub. 116, coefficients for protons and neutrons and heavier ions selected are those calculated by Sato et al. using Particle and Heavy Ion Transport (PHITS; Sato et al., 2003a, 2009, 2010; Niita et al., 2010). The coefficients for lighter particles are calculated from organ dose data initially used to calculate ICRP Pub. 60 effective dose coefficients. (Pelliccioni, 2000; Ferrari et al., 2005). Neither ICRP standard suggests radiation weighting factors for deuterons, tritons, or helions. Based on their similarities to protons and alpha particles with regard to track structure, a radiation weighting factor of two is assigned to deuterons and tritons, while helions are assigned a value of 20, consistent with the ICRP definition of the radiation weighting factor based on mean quality factors for these particles (Sato et al., 2003b; Copeland et al., 2012).

To obtain fluence-to-dose conversion coefficients following ICRP Pub. 60 recommendations for light and heavy ions (deuterons and heavier ions) from those calculated using ICRP Pub. 103 recommendations, the organ dose data calculated by Sato et al. based on ICRP Pub. 103 recommendations were re-weighted using the tissue weighting factors (and radiation weighting factors, if needed) in the ICRP Pub. 60 recommendations (ICRP, 1991; ICRP 2007; Sato et al., 2010). However, in this case, a radiation weighting factor of five was assigned to deuterons and tritons, while helions were again assigned a value of 20.

For ambient dose equivalent H*(10), the coefficients of Pelliccioni (2000) were used when possible: muons, pions, electrons, photons, neutrons, and protons. For other particles, fluence-to-effective dose conversion coefficients based on ICRP Pub. 103 recommendations are used.

Whole-Body Average Absorbed Dose

The fluence-to-whole-body-average-absorbed-dose coefficients provide a means for comparing effective dose to similar quantities such as effective dose equivalent, often favored for space applications, through mean quality factors (National Council on Radiation Protection and Measurement [NCRP], 2000).

Since fluence-to-absorbed dose data must be calculated as an intermediate step to calculate coefficients for fluence-to-effective dose conversion, coefficients are sometimes published along with the fluence-to-effective dose coefficients or made available from the authors by other means such as institutional Websites. For the Sato et al. heavy ion coefficients, organ dose data used by CARI-7 were taken from the JAEA-PHITS Website (phits.jaea.go.jp/ddcc/) while organ data for the coefficients collected by Pelliccioni was kindly provided by Pelliccioni (Sato et al., 2009, 2010; Research Group for Radiation Transport Analysis, 2019; Pelliccioni, 2000, personal communication, 2005).

For each tissue, the average absorbed dose was calculated from the organ dose data using the organ mass data from the male and female Bodybuilder phantoms designed for use in MCNP (Van Riper, 2005). When absorbed dose values were not published, needed organ doses were calculated from the organ-specific fluence-to-effective dose conversion data (M. Pelliccioni, personal communication, 2005; Sato et al., 2010) and the radiation weighting factors.

Ambient Dose Equivalent, H*(10)

The International Commission on Radiation Units and Measurements (ICRU) and the ICRP (1997) define ambient dose equivalent as the dose equivalent measured within a 30-cm diameter sphere of tissue-equivalent material (called the ICRU sphere) irradiated by a plane parallel beam. Since effective dose cannot be measured, but properly calibrated instruments can measure ambient dose equivalent, the latter is sometimes used as a measurement surrogate for effective dose in aviation. Ambient dose equivalents at various depths (d, in mm) along the axis of the sphere opposing the incident radiation beam depth are denoted by H*(d). Thus, H*(10) is the ambient dose equivalent at a depth of 10 mm. Like effective dose, it is also measured in units of joule per kilogram with the special name sievert (Sv). The calculations of coefficients proceed along the same lines as those for effective dose coefficients, except that the anthropomorphic phantoms needed to calculate effective dose are replaced by the ICRU sphere, and the radiation source is a beam of parallel moving particles.

Effective Dose

The ICRP introduced effective dose as a radiation protection quantity in its 1990 recommendations (ICRP, 1991). In its 2007 recommendations, the ICRP continued to recommend effective dose as a radiation

protection quantity for general application, including aviation at high altitudes (ICRP, 2007). The 2007 revisions included a slightly different set of tissue weighting factors and radiation weighting factors for calculating effective dose, and a standard phantom was adopted (ICRP, 2009). Tables of coefficients based on the updated standards were published in Publication 116 (ICRP, 2010).

For CR dosimetry, the most important changes involved neutron and proton radiation weighting factors. Both were generally reduced in the newer recommendations. The proton contribution to effective dose was reduced by 60% (radiation weighting factor reduced from 5 to 2), while the factors for the lowest and highest energy neutrons were also reduced (from 5 to 2.5). The most important change to tissue weighting factors made in the 2007 recommendations was increased breast tissue weighting. Because of this tissue's shallow depth, weakly penetrating particles can more significantly affect the dose under the newer recommendations. As a result, coefficient values rise faster at low energies. At higher particle energies, organ depth is less important, and coefficients from the two sets of tissue weighting factors return to being essentially the same. The net effect is reduced dose rates when using the newer recommendations (Table 5).

Table 5

Effective Doses Using 1990 and 2007 Recommendations of the ICRP and Ambient Dose Equivalent, H(10), Calculated with CARI-7 rel. 4.0.2 at 10.7 km (35,000 ft)*

IGRF 2000 vertical magnetic rigidity cutoff at 20 km / GV	Date	Effective dose rate, 1990 ICRP recommendations / $\mu Sv \cdot h^{-1}$	Effective dose rate, 2007 ICRP recommendations / $\mu Sv \cdot h^{-1}$	Ambient dose equivalent, H*(10) / $\mu Sv \cdot h^{-1}$
0	2002/01	5.33	4.11	4.68
0	1998/01	7.39	5.68	6.57
17	2002/01	1.81	1.44	1.54
17	1998/01	1.91	1.52	1.63

Note. ICRP = International Commission on Radiological Protection

Absorbed Dose in Si and NM-64 Neutron Monitor Tube Response

Coefficients for the absorbed dose in 150-mm by 150-mm by 0.3-mm thickness silicon, 0.5-mm thickness silicon, and neutron monitor response used by CARI-7 were developed for PANDOCA (Matthiä et al., 2014). The coefficient set for dose in 0.5-mm silicon did not contain coefficients for heavy ion, triton, helion, or deuteron data. For these particles, 0.3-mm data were used as surrogate data.

The coefficient set for NM-64 neutron monitor tube response contains no data for particles other than alphas, protons, muons, electrons, pions, and neutrons. Thus, this feature must be used with extreme care, and results should not be trusted if other particles may significantly alter count rates. Results should be normalized to the monitor being simulated.

Vehicle-Related Shielding

Due to the extra computational time required, accounting for aircraft structure was considered impractical and created a needless loss of generality where the structure and contents of the aircraft of eventual application of the data are unknown. This conclusion is supported by studies of the effects of aircraft structure on the dose rate within the aircraft (Battistoni et al., 2005; Foelsche et al., 1974). Battistoni et al. used the FLUktuierende KAskade (FLUKA) to study the effects of aircraft structure on GCR dose at commercial altitudes and found structure and contents could reduce the dose by up to 8%, depending on the location within the cabin. These agree with earlier calculations reported by Foelsche et al., which

suggested the effect of structure on the dose rates inside the cabin would be within 5% to 10% of the dose rate calculated without accounting for the structure at supersonic transport (SST) cruise altitudes (18.3 to 19.8 km, FL 600 to FL 650). Thus, by default, shielding is not accounted for by CARI-7 or CARI-7A.

However, for situations where the aircraft or spacecraft is a significant fraction of the shielding for its occupants (as in spaceflight and extremely high-altitude aircraft), shielding can be included in the calculations. This is currently done in an approximate manner, with three shielding materials currently allowed: dry air, aluminum alloy, and polyethylene. The net effect is the thickness weighted average of the three materials' effectiveness relative to dry air. Reports by Copeland (2017b), Copeland and Atwell (2018), and Atwell et al. (2018) present details of the method of correction.

Uncertainty

Sources of uncertainty in the calculations include the CR primary spectrum, fluence-to-dose conversion coefficients, and MCNPX shower particle fluences. The fluence-to-dose conversion coefficients were calculated with Monte Carlo techniques using MCNPX, PHITS, (Niita et al. 2010), GEometry ANd Tracking 4 (GEANT4; Agostinelli et al., 2003), and FLUKA (Ferrari et al., 2005). Uncertainties were not always provided with the coefficients. Thus, based on a survey of these available uncertainty data, 2.5% was chosen as a conservative estimate for all coefficients. Most of the uncertainty in any calculation comes from the CR model. For CARI-7, uncertainty reporting is turned off. The uncertainties reported by CARI-7A are calculated using assumptions of complete independence of variables, a normal distribution of values, and that individual element uncertainties in GCR were expressed in terms of standard uncertainties, equivalent to standard deviations with respect to combining uncertainties. For the standard International Standards Organization (ISO) GCR model, the uncertainties used are those provided in the published model. For models other than the standard ISO model, the uncertainty is unknown, and a value of 50% has been assigned to each datum from the model. An estimate made by comparing the effective doses for the same location and solar activity conditions at several altitudes (Figure 4) using the four different GCR models (i.e., ISO, Badhwar-O'Neill 2011, Badhwar-O'Neill 2014, and the ISO local interstellar spectrum modulated by heliocentric potential [ISO, 2004; O'Neill and Foster, 2011; O'Neill et al., 2015, Copeland, 2017a]) is about 7%, with the greatest variation at the top of the atmosphere.

Figure 4

ICRP Pub. 103 Effective Doses at Selected Altitudes Calculated for Conditions of Solar Minimum (January 1998) and 0 GV Apparent Cutoff with Each of the Four GCR Models Currently Selectable in CARI-7A.

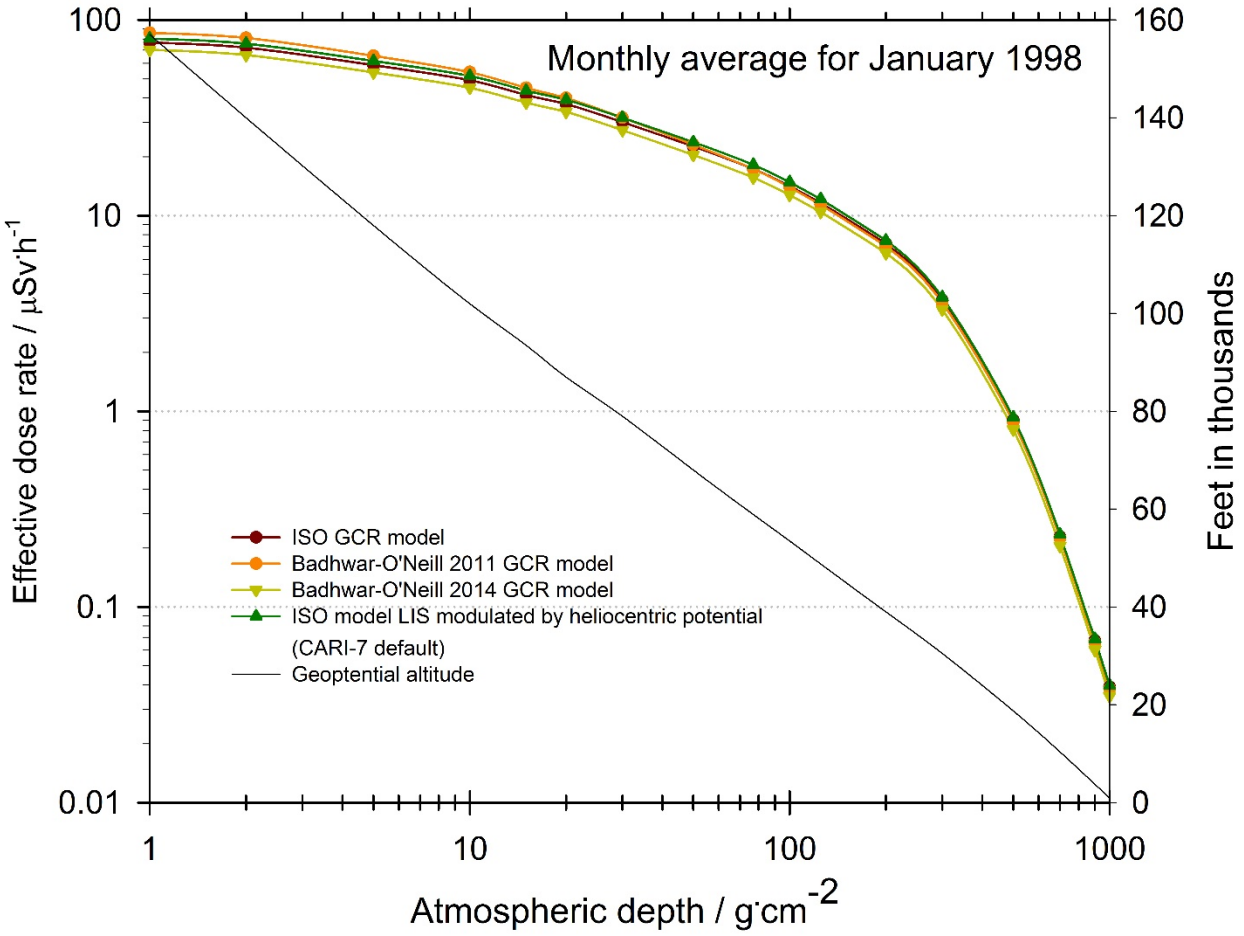

Transport Options

Superposition Approximation

The radiation transport model used to create CARI-6, LUIN2000, approximated the deuterons and heavier ions present in GCR using what is known as the *superposition approximation* to simplify atmospheric transport modeling (O'Brien et al., 2003; Copeland, 2015). The simplest form of the superposition approximation treats CR nuclei with more than one nucleon as multiple free nucleons for atmospheric transport, with the energy per nucleon and rigidity taken from the originating nucleus. For example, an alpha particle (helium nucleus) is treated as two free protons and two free neutrons. The superposition approximation was once commonly used in the transport calculations built into aircrew dosimetry programs. It both greatly simplified the physics models needed for the calculations and vastly reduced the needed number of calculations. Figure 5 shows the effect of superposition on effective dose rates, a dosimetric quantity recommended for use in radiation protection by various organizations such as the ICRP (1991, 2007) and NCRP (1994). The fact that dosimetry programs like CARI-6, which are based on transport models incorporating this approximation, work with good accuracy in the lower and middle atmosphere (where modern commercial and business aviation takes place) is proof that the approach was

highly successful for these regions. It is less successful in the upper atmosphere, where significant numbers of CR heavy ions are present. Until they break up, these ions lose energy due to ionization much faster than their nucleonic constituents (ionization is proportional to the square of the charge). Thus, one can reasonably expect varying amounts of underestimation of dose rates at very high-altitudes and some overestimation of dose rates at very low-altitudes when using superposition.

Figure 5

Ratios of Dose Rates Calculated Using the Superposition Approximation to Those Calculated Without Using the Superposition Approximation

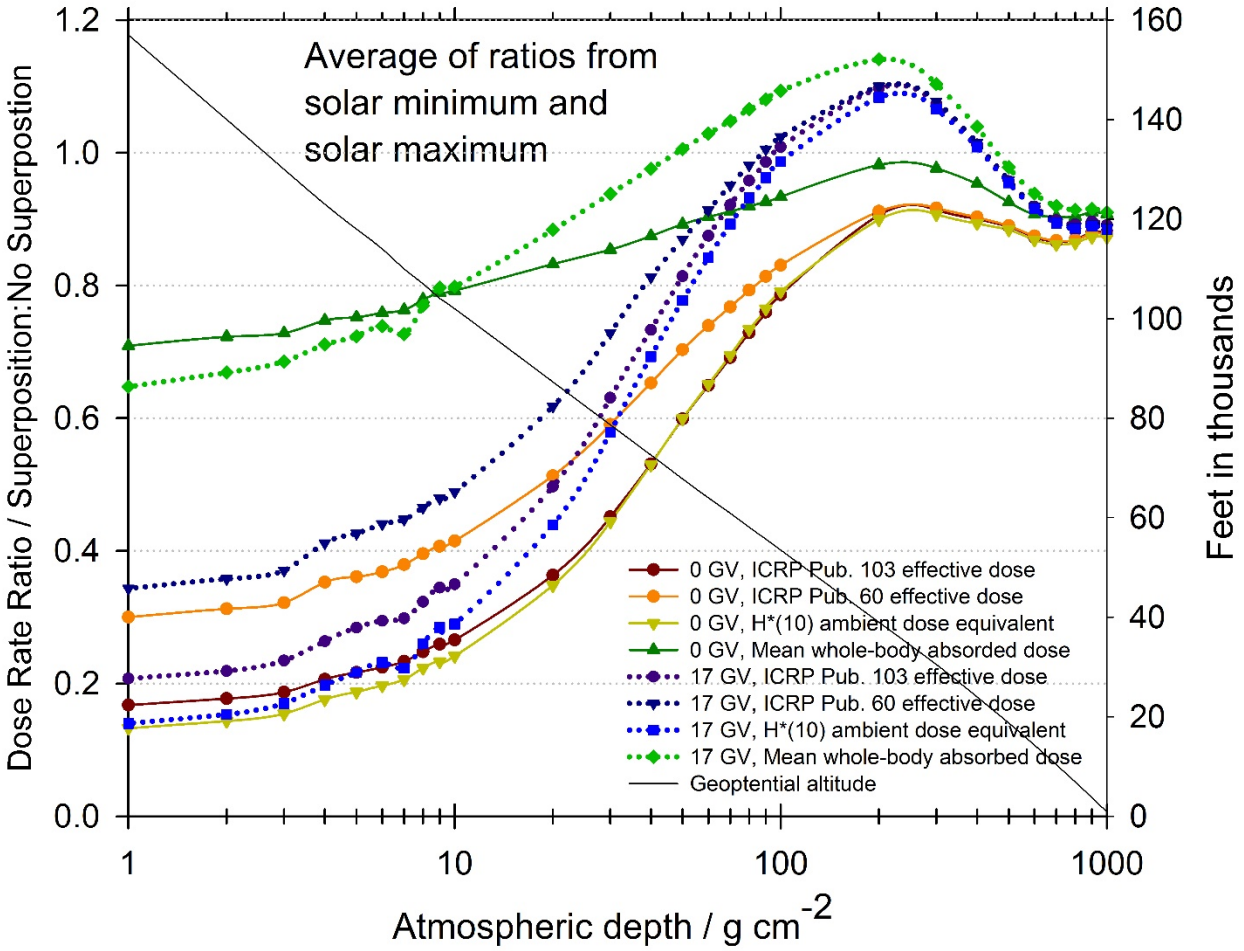

Note. Ratios shown are averages from solar minimum and solar maximum dose rates, calculated using the Badhwar-O'Neill 2011 GCR model in the polar latitude region (0 GV cutoff rigidity) and equatorial latitude (~17 GV cutoff rigidity).

While superposition remains an option in CARI-7A, not using the approximation gives CARI-7 an important advantage over its predecessors in calculating doses and dose rates to occupants of aircraft flying at high altitudes or in spacecraft.

Angularly Resolved Transport

For CARI-7, the most reasonable choices are preselected for the user by the developers (Table 6). For atmospheric transport, this means that radiation showers are assumed to be built from isotropically incident fluences of radiation entering the atmosphere at an altitude of 100 km. The fluence data are handled in a manner most similar to the original MCNPX simulation design, and the superposition approximation is avoided.

Table 6

Options in CARI-7A That Are Preselected and Unchangeable for CARI-7 Users

Option	Setting
GCR model	ISO-HP
Superposition approximation	OFF
Magnetic cutoff rigidities	Use Apparent Cutoff Rigidity
Angularly resolve shower depths	OFF
Vehicle-Related Occupant Shielding	NONE

Note. CARI = Civil Aviation Research Institute; GCR = Galactic cosmic radiation; HP = Heliocentric Potential; ISO = International Standard Organization.

In addition to using the superposition approximation, CARI-7A also allows the user to approximate angularly resolved transport (i.e., handle the data as if transport results were the result of vertical beams at the same tally shell depths); this can be a good approximation at very-large depths, where secondaries from nonvertical primary particles do not contribute much to totals. This can be applied with or without the use of zenith- and azimuth-dependent nonvertical cutoff rigidities. The shower-result integration method reconstructs the total dose from contributions from various slant depths, useful if nonvertical cutoff rigidities are also used directly, rather than an effective or apparent cutoff rigidity (see Copeland, in press-a). When the user requests beam-like transport and/or angularly resolved cutoff rigidities, the sky is subdivided into 900 sections (the number needed to stabilize the results) above the horizon, characterized by azimuth (18 subdivisions) and zenith (50 subdivisions).

Each section's contribution from each primary ion spectrum to the total is considered. With regard to geomagnetic passage into each sector, a pass-band function of primary particle rigidity is used. Each band of a primary ion spectrum with a lower rigidity above the cutoff for that sector is fully allowed, and each band of a primary ion spectrum with an upper rigidity below the cutoff for that sector is wholly rejected. Also, each band of a primary ion spectrum with an upper rigidity above the cutoff for that sector and with a lower rigidity below the cutoff for that sector is only allowed to contribute based on the fluence of that primary ion spectrum within the band with rigidity above the cutoff.

Table 7 shows the results of effective dose calculations from the ISO (2004) GCR model modulated by heliocentric potential (the preselected choice for CARI-7) for each of the five transport options (i.e., options 0–4) available in CARI-7A. The options remain in CARI-7A because they allow the user to probe—to some extent—the sensitivity of the model to using zenith- and azimuth-dependent cutoff rigidities, and the options allows the user to gain some insight into just how useful (or not) the isotropically incident tally data are for approximating results from mono-directionally incident beams at different atmospheric depths. Furthermore, the options remain because the coding can be readily adapted for application to spacecraft shielding evaluation, where no atmosphere is used, and if a suitable transform function was developed, directionally dependent aircraft shielding would also be a natural extension. Finally, while atmospheric

fluences based on beam transport would be needed to get good model results at all depths, when those atmospheric fluences become available, much of the coding will be in place in CARI-7A.

Table 7

Effective Dose Rates at Selected Altitudes Calculated Using Nuclear Transport Near Solar Minimum (January 1998) Using the ISO GCR Model LIS Modulated by Heliocentric Potential[A]

	Vertical Cutoff rigidity = 17 GV				
Depth/ g cm^2	Option 0[A,B]	Option 1	Option 2	Option 3	Option 4
1000	2.32E-02	2.28E-02	3.25E-03	3.31E-03	2.38E-02
900	3.88E-02	3.82E-02	5.98E-03	6.08E-03	4.00E-02
700	9.77E-02	9.72E-02	1.87E-02	1.91E-02	1.02E-01
500	3.13E-01	3.15E-01	6.64E-02	6.81E-02	3.27E-01
300	1.10E+00	1.11E+00	3.05E-01	3.13E-01	1.14E+00
200	1.87E+00	1.91E+00	6.83E-01	7.01E-01	1.95E+00
125	2.45E+00	2.51E+00	1.21E+00	1.24E+00	2.56E+00
85	2.58E+00	2.64E+00	1.44E+00	1.48E+00	2.70E+00
70	2.68E+00	2.76E+00	1.67E+00	1.72E+00	2.82E+00
50	2.82E+00	2.94E+00	1.98E+00	2.05E+00	2.98E+00
30	3.10E+00	3.26E+00	2.29E+00	2.38E+00	3.30E+00
20	3.39E+00	3.58E+00	2.58E+00	2.69E+00	3.62E+00
15	3.45E+00	3.66E+00	2.76E+00	2.89E+00	3.70E+00
10	3.94E+00	4.20E+00	3.05E+00	3.21E+00	4.23E+00
5	4.20E+00	4.50E+00	3.54E+00	3.75E+00	4.52E+00
2	4.84E+00	5.17E+00	4.10E+00	4.37E+00	5.21E+00
1	5.07E+00	5.41E+00	4.53E+00	4.82E+00	5.45E+00

[A] Option 0 is preselected and unchangeable in CARI-7.

[B] Options: 0) Isotropic showers, apparent cutoff rigidity; 1) Isotropic showers, cutoff rigidities dependent on zenith and azimuth from Eq. 1 from Copeland (2017); 2) Shower data treated as beams using Eq. 2 from Copeland (2017), apparent cutoff rigidity; 3) Shower data treated as beams using Eq. 2, cutoff rigidities dependent on zenith and azimuth from Eq. 1 from Copeland (2017); 4) Isotropic showers, effective vertical cutoff rigidity used as apparent cutoff rigidity.

Note. GCR = Galactic cosmic radiation; ISO = International Standard Organization.

CONCLUDING REMARKS

This report describes the methods used in CARI-7 and CARI-7A to calculate dose rates and other quantities of interest resulting from CR entering Earth's atmosphere. Future improvements related to atmospheric radiation transport and fluence-to-dose conversion include:

- Development of beam transport results for improved results with angularly resolved dosimetry in the atmosphere.
- Addition of output options such as effective dose equivalent, absorbed dose in air, other instrument related dosimetric quantities, and particle spectra.
- Recalculation of MCNPX shower data with a more accurate successor (currently, this would be MCNP6).

CARI-7 and CARI-7A were developed with model flexibility in mind. CARI-7 uses what are considered the most reasonable choices for normal aviation dosimetry, while CARI-7A includes additional options allowing the user to explore the sensitivities of results to model choices and is more readily applied to less common uses like spaceflight. All of the transport, geomagnetic, and spectra options influence dose rates in the atmosphere to various degrees and work continues to both verify results and improve usefulness of the programs for all possible applications (e.g., Atwell et al., 2018; Copeland and Atwell, 2018; Matthias et al., 2018).

Some Suggested Readings

For a report focusing on aviation's biological effects, please see *Ionizing Radiation in Earth's Atmosphere and in Space Near Earth. Report DOT/FAA/AM-11/9* by W. Friedberg and K. Copeland, K., published in 2011 by the Federal Aviation Administration Office of Aerospace Medicine.

The interested layperson should consider reading *A Thin Cosmic Rain: Particles from Outer Space* by M. W. Friedlander, published in 2000 by Harvard University Press.

An upper-level college textbook published in 2016 on topics discussed in this report is *Cosmic Rays and Particle Physics, 2nd Ed.* by T. K. Gaisser, R. Engle, and E. Resconi, published by Cambridge University Press.

REFERENCES

Agostinelli, S., Allison, J., Amako, K., Apostolakis, J., Araujo, H., Arce, P., Asai, M., Axen, D., Banerjee, S., Barrand, G., Behner, F., Bellagamba, L., Boudreau, J., Broglia, L., Brunengo, A., Burkhardt, H., Chauvie, S., Chuma, J., Chytracek, R., … Zschiesche, D. (2003). Geant4—a simulation toolkit. *Nuclear Instruments And Methods In Physics Research Section A: Accelerators, Spectrometers, Detectors And Associated Equipment, 506*(3), 250-303. https://doi.org/10.1016/s0168-9002(03)01368-8

Atwell, W., Copeland, K., & Badavi, F. F. (2018, July 8–12). *Geomagnetically-trapped and galactic cosmic radiation environments and absorbed dose calculations for a hypothetical sounding rocket trajectory.* 49th International Conference on Environmental Systems, Boston, MA, United States. https://ttu-ir.tdl.org/handle/2346/84502

Battistoni, G., Ferrari, A., Pelliccioni, M., & Villari, R. (2005). Evaluation of the doses to aircrew members taking into consideration the aircraft structures. *Advances in Space Research, 36*, 1645-1652.

Copeland, K. A. (2014). *Cosmic ray particle fluences in the atmosphere resulting from primary cosmic ray heavy ions and their resulting effects on dose rates to aircraft occupants as calculated with MCNPX 2.7.0*. Doctoral thesis, Royal Military College of Canada (RMCC). Massey Library Collection at RMCC and the Canadian National Archives in Ottawa, Canada.

Copeland, K. (2015). Influence of the superposition approximation on calculated effective dose rates from galactic cosmic rays at aerospace-related altitudes. *Space Weather, 13*(7), 401-405. https://doi.org/10.1002/2015SW001210.

Copeland, K. (2017a). CARI-7A: Development and Validation. *Radiation Protection Dosimetry, 175*(4), 419-431. https://doi.org/10.1093/rpd/ncw369

Copeland, K. (2017b). *Approximating Shielding Effects on Calculations of Effective Dose Rate from Galactic Cosmic Radiation during Extreme Altitude and Suborbital Flights using CARI-7*. Federal Aviation Administration Office of Aerospace Medicine Report DOT/FAA/AM-17/8. https://rosap.ntl.bts.gov/view/dot/37291

Copeland, K. (2020). *CARI-7 Documentation: Geomagnetic Cutoff Rigidity Calculations and Tables for 1965-2010*. Federal Aviation Administration Office of Aerospace Medicine Report DOT/FAA/AM-19/4, Federal Aviation Administration Office of Aerospace Medicine.

Copeland, K. (2021). *CARI-7 Documentation: Particle Spectra*. Federal Aviation Administration Office of Aerospace Medicine Report DOT/FAA/AM-21/4, Federal Aviation Administration Office of Aerospace Medicine.

Copeland, K., & Atwell, W. (2018, July 8–12). *Influence of aircraft self-shielding on worldwide calculations of effective dose rates to occupants*. 48th International Conference on Environmental Systems. Albuquerque, NM, United States. https://ttu-ir.tdl.org/handle/2346/74225

Copeland, K., Friedberg, W., Sato, T., & Niita, K. (2012). Comparison of fluence-to-dose conversion coefficients for deuterons, tritons, and helions. *Radiation Protection Dosimetry, 148*(3), 344-351, https://doi.org/10.1093/rpd/ncr035

Copeland, K., Sauer, H. H., Duke, F. E., & Friedberg, W. (2008). Cosmic radiation exposure of aircraft occupants on simulated high-latitude flights during solar proton events from 1 January 1986 through 1 January 2008. *Advances in Space Research, 42*(6), 1008-1029.

Ferrari, A. & Pelliccioni, M. (2003). On the conversion coefficients for cosmic ray dosimetry. *Radiation Protection Dosimetry, 104(3)*, 211-220.

Ferrari, A., Sala, P. R., Fasso, A., Ranft, J., & Siegen. U. (2005). *FLUKA: A Multi-Particle Transport Code*. https://doi.org/10.2172/877507

Foelsche, T., Mendell, R. B., Wilson, J. W., & Adams, R. R. (1974). *Measured and Calculated Neutron Spectra and Dose Equivalent Rates at High Altitudes; Relevance to SST Operations and Space Research*. Report No. NASA TN D-7715. National Aeronautics and Space Administration.

Friedberg, W., & Copeland, K. (2011). *Ionizing Radiation in Earth's Atmosphere and in Space Near Earth*. Report DOT/FAA/AM-11/9, Federal Aviation Administration Office of Aerospace Medicine.

Friedlander, M. W. (2000). *A thin cosmic rain: Particles from outer space*. Harvard University Press.

Gaisser, T. K., Engle, R., & Resconi, E. (2016). *Cosmic rays and particle physics, 2nd Ed.* Cambridge University Press.

International Commission on Radiological Protection. (1991). *1990 Recommendations of the International Commission on Radiological Protection.* ICRP Publication 60. *Annals of the ICRP, 21*, 1-3.

International Commission on Radiological Protection. (1997). *Conversion Coefficients for use in Radiological Protection against External Radiation*. ICRP Publication 74. *Annals of the ICRP, 26*, 3-4.

International Commission on Radiological Protection. (2007). *The 2007 Recommendations of the International Commission on Radiological Protection*. ICRP Publication 103. *Annals of the ICRP, 37*, 2-4.

International Commission on Radiological Protection. (2009). *Adult reference computational phantoms.* ICRP Publication 110. *Annals of the ICRP, 39*, 2.

International Commission on Radiological Protection. (2010). *Conversion coefficients for radiological protection quantities for external radiation exposure.* ICRP Publication 116. *Annals of the ICRP, 40,* 2-5.

International Commission on Radiation Units and Measurements. Reference Data for the Validation of Doses from Cosmic-Radiation Exposure of Aircraft Crew. ICRU Report 84. *Journal of the ICRU*, *10*(2).

International Standards Organization. (2004). *Space environment (natural and artificial) -- Galactic cosmic ray model*. ISO TS 15930:2004. Retrieved June 12, 2013 from www.iso.org/iso/home/store/catalogue_tc/catalogue_detail.htm?csnumber =37095&commid=46614

Lei, F., Hands, A., Truscott, P., & Dyer, C. (2009). *Cosmic-ray Heavy Ions Contributions to the Atmospheric Radiation Field*. 2009 European Conference on Radiation and Its Effects on Components and Systems (RADECS). https://doi.org/10.1109/RADECS.2009.5994679

Matthiä, D., M. M. Meier, & Reitz G. (2014). Numerical calculation of the radiation exposure from galactic cosmic rays at aviation altitudes with the PANDOCA core model. *Space Weather, 12,* 161–171. https://doi.org/10.1002/2013SW001022.

Matthias M. M., Copeland, K., Matthiä, D., Mertens, C. J., & Schennetten, K. (2018). First steps towards the verification of models for the assessment of the radiation exposure at aviation altitudes. *Space Weather, 16*(9), 1269-1276 https://doi.org/10.1002/2018SW001984

National Aeronautics and Space Administration. (1999). ACE abundance data to plot. Retrieved March 2, 2014 from helios.gsfc.nasa.gov/ace/abund_plot.html

National Aeronautics and Space Administration (2010). *Layers of Earth's Atmosphere*. https://www.nasa.gov/topics/solarsystem/sunearthsystem/atmospheric-layers.html

National Aeronautics and Space Administration (2012a). World book at NASA. Retrieved April 3, 2012 from www.nasa.gov/worldbook/meteor_worldbook.html.

National Aeronautics and Space Administration (2012b). Space math @ NASA problem 185: The International Space Station: follow that graph! Retrieved April 3, 2012 from spacemath.gsfc.nasa.gov/weekly/5Page35.pdf.

National Center for Atmospheric Research & the University Corporation for Atmospheric Research (UCAR) Office of Programs. (2003). The Layered Atmosphere. Retrieved October 8, 2020 from eo.ucar.edu/basics/wx_1_b.html

National Council on Radiation Protection and Measurements. (2000). *Fluence-Based and Microdosimetric Event- Based Methods for Radiation Protection in Space*. NCRP Report 137.

National Oceanic and Atmospheric Administration, National Aeronautics and Space Administration, & United States Air Force. (1976). *U.S. Standard Atmosphere, 1976*. NOAA-S/T 76-1562.

Niita, K., Matsuda, N., Iwamoto, Y., Iwase, H., Sato, T., Nakashima, H., Sakamoto, Y., & Sihver, L. (2010). PHITS: Particle and Heavy Ion Transport code System, Version 2.23. JAEA-Data/Code 2010-022.

Oak Ridge National Laboratory. (2011). *Monte Carlo N-Particle Transport Code System for Multiparticle and High Energy Applications (MCNPX 2.7.0), RSICC code package C740*. Los Alamos National Laboratory.

O'Brien, K., Smart, D. F., Shea, M. A., Felsberger, E., Schrewe, U., Friedberg, W., & Copeland K. (2003). Worldwide radiation dosage calculations for air crew members. *Advances in Space Research, 31*(4), 835–840.

O'Neill P. M. & Foster C. C. (2013). *Badhwar-ONeill 2011 Galactic Cosmic Ray Flux Model Description*. Tech. Rep. NASA/TP-2013-217376.

O'Neill P. M., Gogle, S., & Slaba, T. C. (2015). *Badhwar-ONeill 2014 Galactic Cosmic Ray Flux Model Description*. Tech. Rep. NASA/TP-2015-218569.

Pelliccioni, M. (2000). Overview of fluence-to-effective dose and fluence-to-ambient dose equivalent conversion coefficients for high energy radiation calculated using FLUKA code. *Radiation Protection Dosimetry, 88*(4), 279–297.

Research Group for Radiation Transport Analysis. (n.d.). *DDCC Databases of Dose Conversion Coefficients Homepage*. Retrieved July 29, 2019, from https://phits.jaea.go.jp/ddcc/

Sato, T., Tsuda, S., Sakamoto, Y., Yamaguchi, Y., & Niita, K. (2003a). Conversion coefficients from fluence to effective dose for heavy ions with energies up to 3 GeV/A. *Radiation Protection Dosimetry*, *106*, 137-144.

Sato, T., Tsuda, S., Sakamoto, Y., Yamaguchi, Y., & Niita, K. (2003b). Analysis of dose-LET distribution in the human body irradiated by high energy hadrons. *Radiation Protection Dosimetry*, *106*, 145-153.

Sato, T., Endo, A., Zankl, M., Petoussi-Henss, N., & Niita, K. (2009). Fluence-to-dose conversion coefficients for neutrons and protons calculated using the PHITS code and ICRP/ICRU adult reference computational phantoms. *Physics in Medicine and Biology, 54*(7), 1997–2014. https://doi.org/10.1088/0031-9155/54/7/009

Sato, T., Endo, A., & Niita, K. (2010). Fluence-to-dose conversion coefficients for heavy ions calculated using the PHITS code and the ICRP/ICRU adult reference computational phantoms. *Physics in Medicine and Biology, 55*(8), 2235–2246. https://doi.org/10.1088/0031-9155/55/8/008

Stern D. P. & Peredo, M. (2005). #33 Cosmic Rays. Retrieved May 14, 2019 from www-spof.gsfc.nasa.gov/Education/wcosray.html

Van Riper, K. (2005). *BodyBuilder users guide*. White Rock Science.

Walt, M. (1994). *Introduction to geomagnetically trapped radiation*. Cambridge University Press.

APPENDICES

Appendix A: Layers of Earth's Atmosphere

Earth's atmosphere is retained by gravity. The content (percent by volume) of the atmosphere (dry air) is approximately 78% nitrogen, 21% oxygen, 0.93% argon, and an average of 0.034% carbon dioxide with trace amounts of other gases (e.g., water vapor).

From lower to higher, atmospheric layers are called the *troposphere*, *stratosphere*, *mesosphere*, *thermosphere*, and *exosphere*. With an increase in altitude, temperatures decrease in the troposphere, increase in the stratosphere, decrease in the mesosphere, and increase in the thermosphere. Boundary layers between these zones are called the *tropopause*, *stratopause*, *mesopause*, and *thermopause*, respectively. This structure is illustrated in Figure A1.

Figure A1

The Different Layers of Earth's Atmosphere

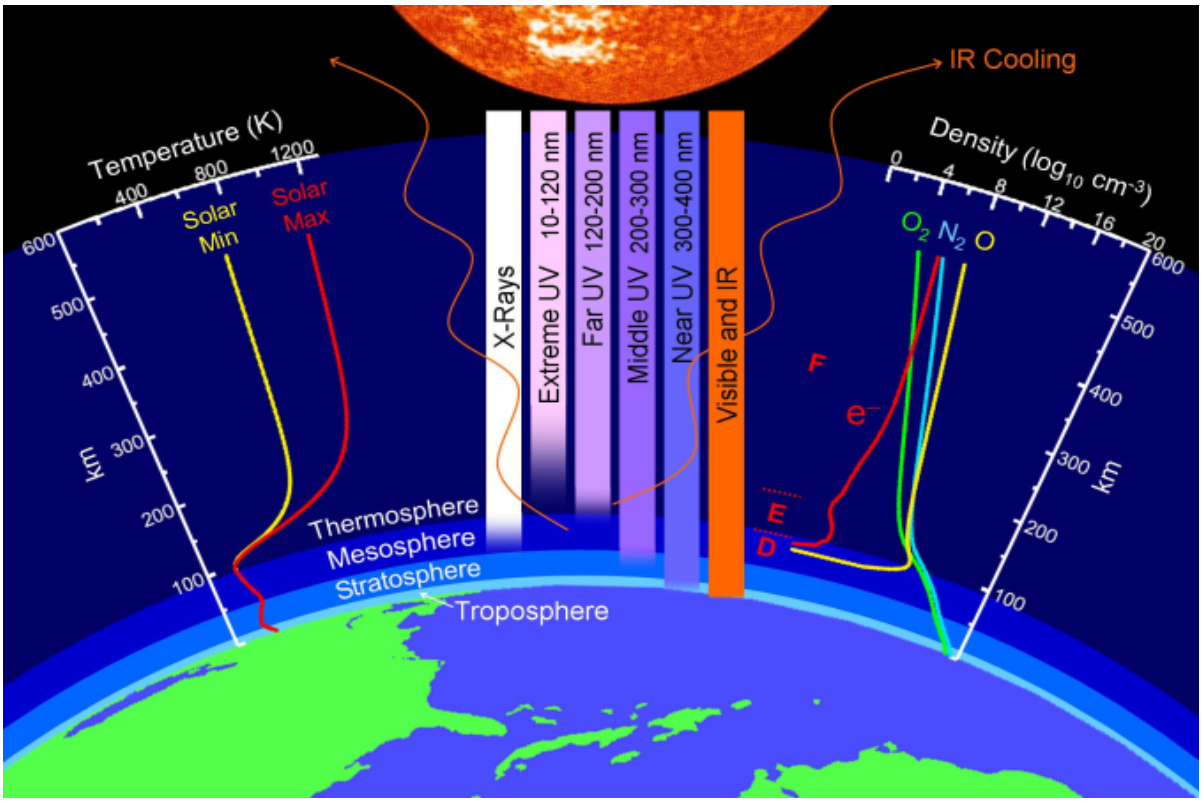

Note. From *Layers of Earth's Atmosphere*, by National Aeronautics and Space Administration, 2010. Credit: John Emmert/Naval Research Lab. https://www.nasa.gov/topics/solarsystem/sunearthsystem/atmospheric-layers.html. UV = ultraviolet; IR = infrared. Thicknesses are approximate, varying worldwide and seasonally.

The *troposphere* extends from the surface to 8 to 10 km near the poles and 16 to 18 km in the tropical regions, with some variation due to weather conditions. It contains most of the atmosphere's mass, and it is where most daily weather occurs observable from the ground. Most commercial aircraft fly at altitudes of 6 to 13 km (20,000 to 42,000 ft), while some charter and executive jet aircraft are capable of 16

km (51,000 ft). The Concorde cruised at 14 to 18 km (45,000 to 60,000 ft). In the *tropopause,* air ceases to cool with height, and it is almost completely dry.

The *stratosphere* extends from the troposphere to about 50 km. The ozone and oxygen in the stratosphere absorb much of the Sun's ultraviolet (UV) radiation. UV radiation can be very harmful to living tissues.

The *stratopause* is the level of transition between the stratosphere and the mesosphere.

The *mesosphere* extends from 50 km to 85 km. Of the millions of meteors that enter Earth's atmosphere every day, most become visible between 65 and 120 km above the Earth and disintegrate at altitudes of 50 to 95 km (NASA, 2012a).

The *mesopause* is the level of transition between the mesosphere and the thermosphere.

The *thermosphere* extends from 80 to 85 km to more than 500 km. The International Space Station orbits Earth at an altitude of 330 to 400 km in the thermosphere (NASA, 2012b).

The *exosphere*, the highest atmospheric layer, is where Earth's atmosphere merges with interplanetary space. In this region, the probability of interatomic collisions is so low that some atoms traveling upward have enough velocity to escape Earth's gravity.

The *ionosphere* contains both ions and neutral molecules and extends from about 80 km to 480 km. Thus, the ionosphere typically overlaps the thermosphere and exosphere, and it is considered the inner edge of the magnetosphere—the region around Earth influenced by Earth's magnetic field (geomagnetic field; Walt, 1994). The ionosphere is used to reflect radio signals over long distances, and it is where aurorae occur.